metals

MDPI

Article

Utilization of a Porous Cu Interlayer for the Enhancement of Pb-Free Sn-3.0Ag-0.5Cu Solder Joint

Nashrah Hani Jamadon [1], Ai Wen Tan [1], Farazila Yusof [1,*], Tadashi Ariga [2], Yukio Miyashita [3] and Mohd Hamdi [1]

[1] Centre of Advanced Manufacturing and Material Processing (AMMP), Department of Mechanical Engineering, University of Malaya, Kuala Lumpur 50603, Malaysia; nashrahhani@gmail.com (N.H.J.); aiwen_2101@hotmail.com (A.W.T.); hamdi@um.edu.my (M.H.)

[2] Department of Metallurgical Engineering, Tokai University, Hiratsuka 259-1292, Japan; ttariga@keyaki.cc.u-tokai.ac.jp

[3] Department of Mechanical Engineering, Nagaoka University of Technology, Nagaoka 940-2188, Japan; miyayuki@mech.nagaokaut.ac.jp

* Correspondence: farazila@um.edu.my; Tel.: +603-796777633; Fax: +603-79675317

Academic Editor: Ana Sofia Ramos

Received: 29 June 2016; Accepted: 5 September 2016; Published: 15 September 2016

Abstract: The joining of lead-free Sn-3.0Ag-0.5Cu (SAC305) solder alloy to metal substrate with the addition of a porous Cu interlayer was investigated. Two types of porous Cu interlayers, namely 15 ppi—pore per inch (P15) and 25 ppi (P25) were sandwiched in between SAC305/Cu substrate. The soldering process was carried out at soldering time of 60, 180, and 300 s at three temperature levels of 267, 287, and 307 °C. The joint strength was evaluated by tensile testing. The highest strength for solder joints with addition of P25 and P15 porous Cu was 51 MPa (at 180 s and 307 °C) and 54 MPa (at 300 s and 307 °C), respectively. The fractography of the solder joint was analyzed by optical microscope (OM) and scanning electron microscopy (SEM). The results showed that the propagation of fracture during tensile tests for solder with a porous Cu interlayer occurred in three regions: (i) SAC305/Cu interface; (ii) inside SAC305 solder alloy; and (iii) inside porous Cu. Energy dispersive X-ray spectroscopy (EDX) was used to identify intermetallic phases. Cu_6Sn_5 phase with scallop-liked morphology was observed at the interface of the SAC305/Cu substrate. In contrast, the scallop-liked intermetallic phase together with more uniform but a less defined scallop-liked phase was observed at the interface of porous Cu and solder alloy.

Keywords: porous Cu interlayer; Sn-3.0Ag-0.5Cu solder alloy; joint strength; fracture morphology

1. Introduction

At present, solder is widely used in the semiconductor packaging industry with the purpose of providing electronic connection. It also plays an important role in the joining of metal components in the transportation, aerospace and energy industries [1–3]. Driven by miniaturization and increased requirements for advanced electronic devices, it is crucial to develop a solder alloy that can remain stable under extreme environments and perform well under high temperature operating systems [4]. Thus, the characteristic performance of the solder alloys is critical since a good quality solder joint could ultimately determine the effective function and reliability of a semiconductor device.

Due to health and environmental concerns, the use of lead-free (Pb-free) solders has been proposed to substitute the lead containing solders in the electronic packaging process [5,6]. To date, Sn-3.0Ag-0.5Cu (SAC305) solder alloy has been proposed as a promising alternative to replace the lead containing solder alloys in electronic applications due to its favourable mechanical properties including superior resistance to creep and thermal fatigue [3,7,8]. This solder is generally applied in commercial

microelectronic devices where the operating temperature usually does not exceed 260 °C. However, due to the higher melting temperature of SAC305 solder alloy (217 °C) compared to the conventional Sn-Pb solder alloy (183 °C), SAC305 solder alloy is thus more viable for middle-temperature-ranged applications [9].

Several studies using SAC305 solder alloy in the electronics assemblies operated at higher temperature have been successfully reported. In a Chellvarajoo et al. study, they reengineered the composite SAC305 solder alloy by adding nanoparticles to enhance the reliability of the solder joint. They found the intermetallic compound (IMC) growth stunted by increasing the percentage of nanoparticles of iron nickel oxide (Fe_2NiO_4) or nickel oxide (NiO) in the SAC305 solder matrix [10,11]. In addition, attempts have also been made in improving the solderability of SAC305 solder alloy in high temperature electronic applications by altering the joining methods through the utilization of an interlayer material in the soldering process, such as during the transient liquid phase (TLP) bonding process. TLP bonding is an established joining technique for die attach bonding in the application of high temperature electronic systems [2]. Generally, a thin layer of low melting point metal is utilized as the interlayer material for an effective bonding during the TLP process. Liu et al. study reported enhanced joint strength and restrained formation of the IMC layer was observed through the use of a composite preform consisting of an Ag based metal core layer with Sn-Ag based solder layers at both sides during the TLP bonding process [12].

More recently, it has been reported that lead-free solder alloys containing additional metal elements have decreased the melting temperature and improved the tensile strength of the solder joints. This was successfully accomplished by adding Cu nanoparticles into Sn-Ag solder alloys [13]. The examination of interfacial interaction during the soldering process showed that Cu particles were dissolved in the solder alloys and this influenced the chemical structure of the Sn-Ag solders, leading to lower melting temperatures and an increase in the solder joint strength. As a result of this promising finding, few studies have been reported to adopt similar techniques for various lead-free solders.

Furthermore, some achievement with enhanced joint quality was also found in the studies through the utilization of porous metal interlayer during the joining process in the field of metal-joining application. Recently, porous metal interlayers have been widely used in various engineering designs such as cooling electronic systems and in aerospace facilities due to its porosity, thermal conductivity and usage efficiency [14–16]. The pores in the porous metal interlayer is reported to assist during the residual stress absorption, which endows this unique feature a remarkable advantage for metal joining applications [17].

For instance, Zaharinie et al. investigated the addition of a porous Cu/Ni interlayer sandwiched in between the sapphire and inconel that were joined using vacuum brazing. The results showed that the Cu/Ni porous composite in the sapphire-inconel joint altered the thermodynamic activity near the ceramic portion of the sapphire, leading to the ductile IMC formation which further improved the joining characteristics [18]. Previously, we have worked on the utilization of porous Cu interlayer in the soldering process where the IMC growth and formation was affected by the porosity of the porous Cu [19]. However, the results are preliminary and warrant further in-depth studies. Since this technique is still in its infancy in the field of soldering technique for electronic assembly application, in this paper, we aim to investigate the influence of porous Cu on its joint strengths, fracture morphologies and the IMC formation. Therefore, modifying the physical soldering process of SAC305 solder alloy through the incorporation of a porous Cu interlayer in the soldering configuration was attempted.

In this paper, the effects of a porous Cu interlayer on the mechanical properties and microstructure of SAC305 solder joints were investigated. We hypothesized the porous Cu interlayer to function as a metal foam allowing the molten solder alloy to penetrate into its internal porous structure to achieve a better joint quality [20].

2. Experimental Procedure

2.1. Material Selection

The SAC305 solder paste alloy material used was provided by Nihon Handa Co., Ltd. (Tokyo, Japan). The chemical composition and general properties of the solder material are given in Tables 1 and 2 [21], respectively. Two types of open cells foam, namely porous Cu interlayer of 15 pore per inch (ppi) and 25 ppi, signified as P15 and P25, were used as the solder joint reinforcement. The interlayer porosity was determined using the mass displacement equation with water as the immersing medium as shown in Figure 1. The percentage of porosity was calculated by the following equation from Archimedes' principle:

$$P(\%) = \frac{W_{as} - W_d}{W_{as} - W_s} \quad (1)$$

where P is the percentage of porosity, W_{as} the weight of porous Cu after submerged in water, W_d represents the weight in dry condition, and W_s the weight of porous Cu while submerged in water. Note that the volume of water displaced is equal to the volume of the porous Cu being submerged. The solid part in the porous Cu is called solid cell walls (SCW) [22].

Table 1. Chemical composition of solder alloy (wt. %).

Solder Alloy	Cu	Ag	Bi	Fe	As	Ni	Pb	Sb	Sn
Sn-3.0Ag-0.5Cu	0.516	3.083	0.011	0.002	0.005	0.001	0.022	0.015	Bal.

Table 2. Mechanical properties of SAC305 [21].

Solder Alloy	Melting Temperature, °C	Tensile Strength, MPa	Young Modulus, MPa	Hardness, HV
Sn-3.0Ag-0.5Cu	217	50.6	54	13.3

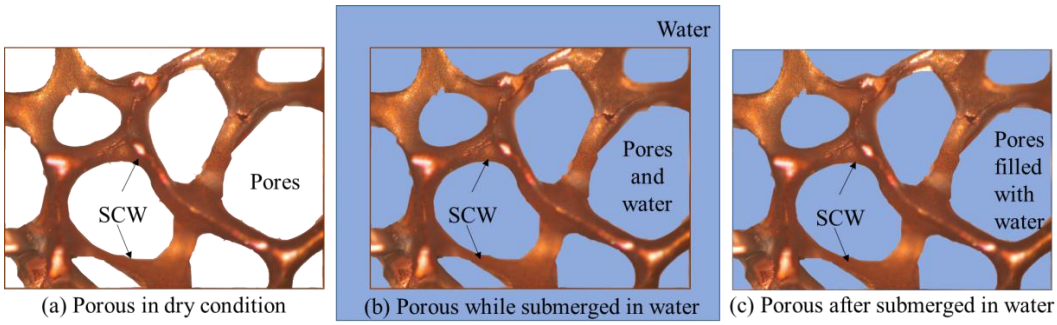

Figure 1. Archimedes' technique to calculate porosity of porous Cu interlayer. (**a**) Porous in dry condition; (**b**) porous while submerged in water; (**c**) porous after submerged in water.

2.2. Joining Procedure and Soldering Process Set Up

Two Cu cylindrical rods with dimensions of 30 mm in length and 8 mm in diameter were used as the substrates. They were soldered together using 0.1 g of SAC305 solder alloy with porous Cu in between the solder alloy, as configured in Figure 2. Prior to the soldering process, the porous Cu interlayers (P15 and P25) were rolled manually with a solid cylinder to obtain a uniform layer with 100 µm in thickness. The solder joint without porous Cu was prepared as a control specimen. The prepared specimen was clamped using a fabricated jig to hold the sample during the soldering process in the tube furnace, as shown in Figure 3. The tube furnace was set up in accordance with the Japanese Industrial Standard, JIS Z 3191. Briefly as shown in Figure 4, the specimen was heated

inside a movable tube furnace under Argon gas atmosphere at a predefined temperature and time. The soldering process was conducted at temperatures of 267, 287, and 307 °C, with three different holding times of 60, 180, and 300 s as listed in Table 3.

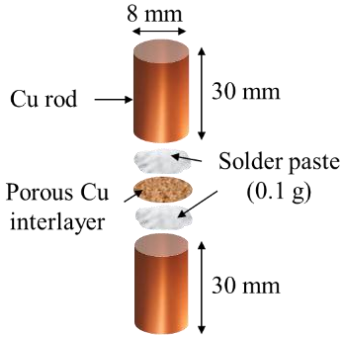

Figure 2. Configuration of a solder joint.

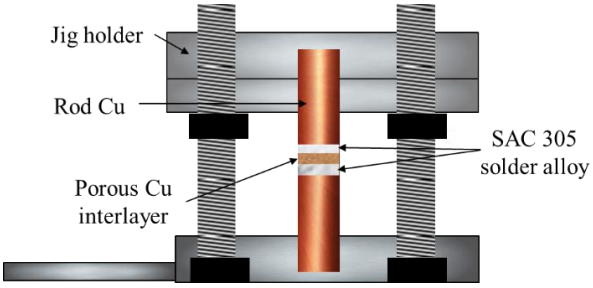

Figure 3. Assembled solder joint at fabricated jig.

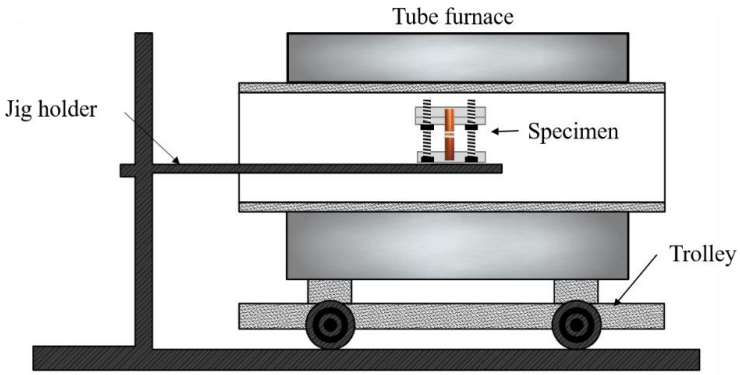

Figure 4. Schematic view of furnace set up as in Japanese Industrial Standard, JISZ 3191.

Table 3. Parameters setting for mechanical testing.

Parameters	Setting Value
Soldering temperature, °C	267, 287, 307
Soldering time, s	60, 180, 300
Porous Cu	0, P15, P25

2.3. Joint Strength Analysis

The strength of the solder joint was measured by tensile testing. The tensile test was carried out at room temperature using Instron® Corporation Universal Testing machine (Model No. 3369, Norwood, MA, USA), with crosshead speed of 0.5 mm/min. The specimen was initially machined at the testing

section to avoid the effect of difference in edge shape caused by over flowing of molten solder during the soldering process. The results of this tensile strength were determined by the average value of three different samples for each condition.

2.4. Microstructural Analysis

After the soldering process, the microstructural observations of the fractured surface were observed under the optical microscope (OM, Olympus, Tokyo, Japan). The cross sections of the soldered joints were also prepared using standard metallorgraphical procedures (sectioning, grinding and polishing) for microstructural analysis. The elemental compositions of the IMC layer were analyzed using scanning electron micrograph (SEM, Crest System (M) Sdn. Bhd., Eindhoven, The Netherlands) equipped with energy dispersive X-ray spectroscopy (EDX, Crest System (M) Sdn. Bhd., Eindhoven, The Netherlands). The fractography (surface and cross section) of the solder joint after the tensile test was also examined by SEM and EDX to study their failure behaviour.

3. Results and Discussion

3.1. Verification of Porosity Percentage

Porous Cu interlayer is characterized by the size of the pore diameter which associates with the porosity [23]. The percentages of the porosity are presented in Figure 5, both experimentally and theoretically. The experimental value was measured by Archimedes' technique, while the theoretical value was calculated by the pore density formula. Figure 6 shows the surface structure of P15 and P25 porous Cu in its pre-rolled and post-rolled conditions. The average thickness of the porous Cu solid cell walls for P15 and P25 porous Cu was 0.23 mm and 0.06 mm, while the pore diameters for P15 and P25 after rolling were 0.3 mm and 0.1 mm, respectively. This showed that the pores were still distinct in shape even after being rolled into a very thin layer. The reason for rolling the porous Cu into a very thin layer was to reduce the joint gap and thereby promote a homogeneous joint layer. In fact, thick joints tend to reduce the joint strength [24].

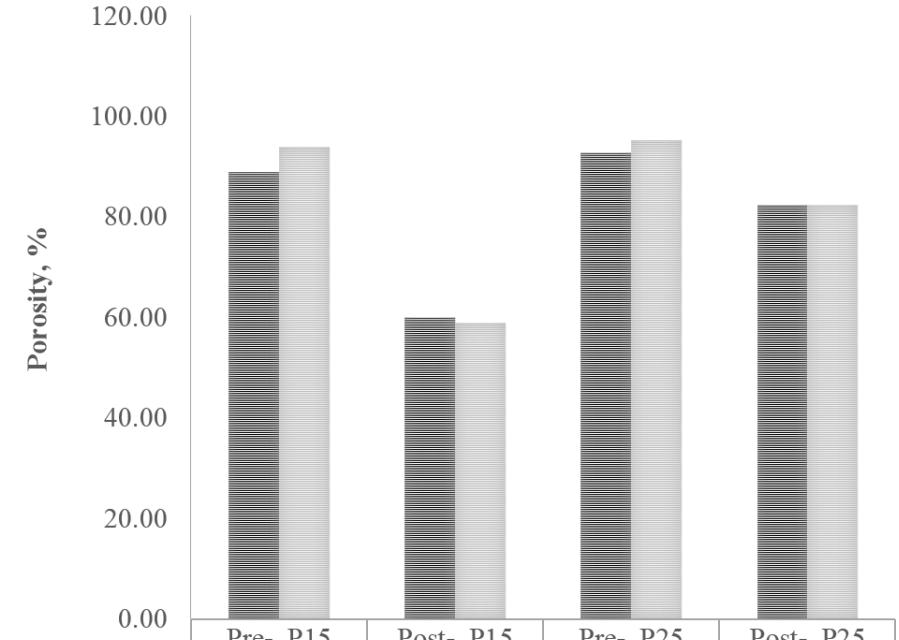

	Pre-, P15	Post-, P15	Pre-, P25	Post-, P25
Experimental	88.83	60.13	92.82	82.31
Theoretical	93.92	58.85	95.24	82.42

Figure 5. Experimental and theoretical measurement of porosity percentage of porous Cu interlayer.

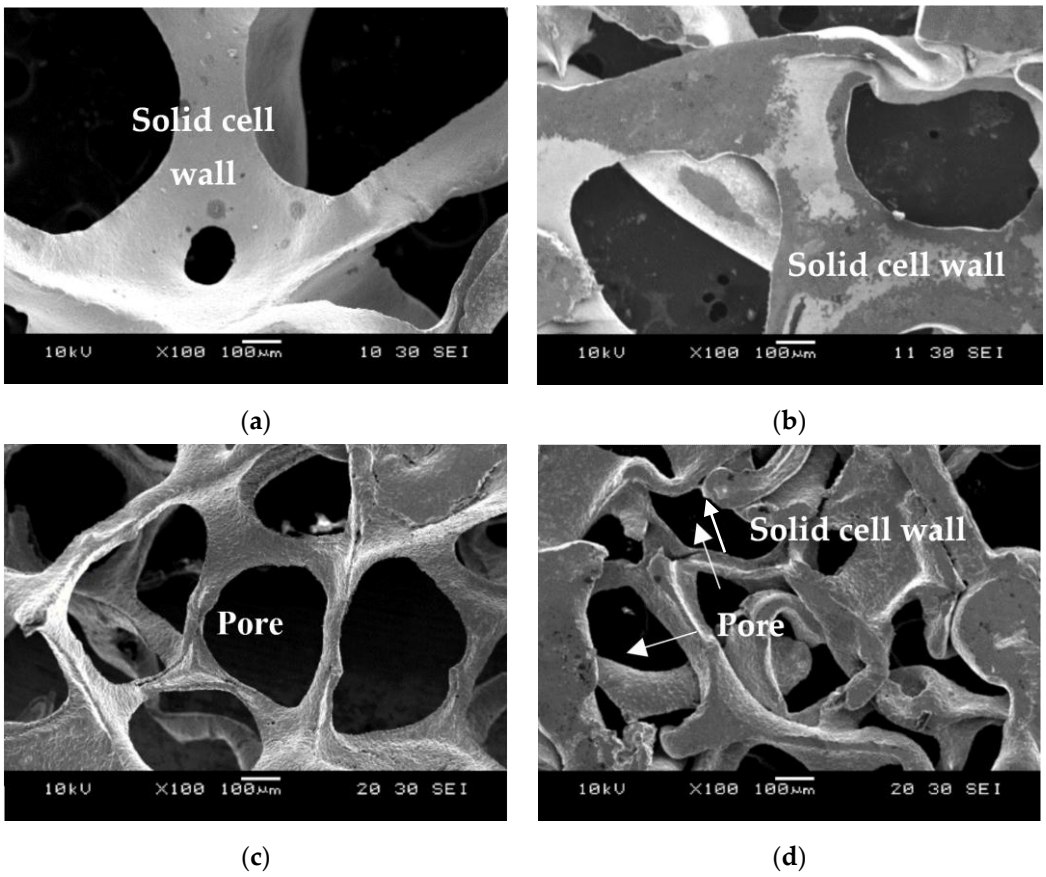

Figure 6. Structure of porous Cu interlayer of P15 and P25 before and after rolling. (**a**) P15, pre-rolled; (**b**) P15, post-rolled; (**c**) P25, pre-rolled; (**d**) P25, post-rolled.

3.2. Effect of Porous Cu Interlayer Addition on Joint Strength

Figure 7 shows the effect of soldering time on joint strength at three different temperatures of solder joint, with and without the two types of porous Cu interlayer. For the control sample without porous Cu, it was observed that the effect of soldering time and temperature on joint strength was minimal as similar joint strength values were recorded for all solder joints, ~40 MPa. In contrast, with the porous Cu addition samples, increasing the soldering time and temperature generally increased the joint strength of the solder joint. In addition, the joint strength of P25 porous Cu solder samples seemed higher compared to the samples with P15 porous Cu at each applied soldering time and temperature; with the exception for P15 porous Cu at soldering time of 60 s and 300 s and temperature of 307 °C. This is possibly due to the effect of differential reaction of porous Cu interface with molten solder in order to create bonding. Only a slight drop in the joint was observed for the P25 porous Cu sample when temperature increased from 287 °C to 307 °C.

The highest strength for the P25 porous Cu addition sample was recorded at 51 MPa with soldering time of 180 s and temperature of 307 °C, whereas, for the sample with P15 porous Cu addition, 54 MPa marked the highest observed strength at soldering time of 300 s and temperature of 307 °C. Both values are acceptable for the optimum joint strength of solder joint for the usage of electronics devices [25]. These values are, in fact, comparable to the joint strength of die attach using composite preform layer during joining as reported in Liu et al. study [12].

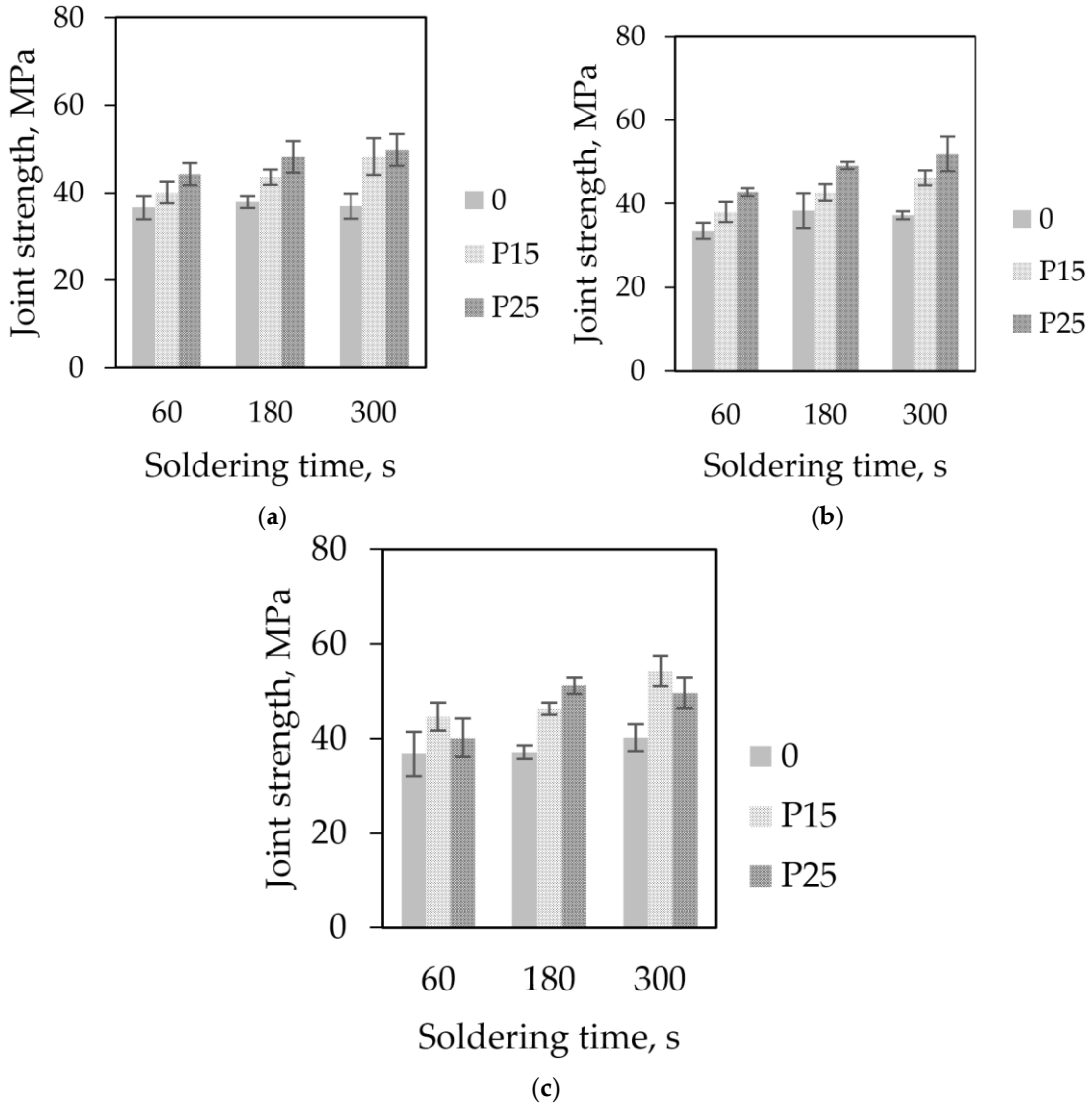

Figure 7. Effect of soldering time and porosity on joint strength at soldering temperature of (**a**) 267 °C; (**b**) 287 °C; and (**c**) 307 °C.

3.3. Effect of Porous Cu Interlayer Addition on Fracture Behaviour

3.3.1. Fractured Surface

The specimens at soldering temperature of 307 °C and 300 s were selected for the microstructure analysis due to the promising results obtained in the joint strength evaluation. The fractured surfaces of both samples, (control and with porous Cu interlayer) are illustrated in Figure 8a–c, while high magnification images of the selected area are shown in Figure 8d–f. The fracture of the solder joint without porous Cu interlayer occurred in between the Cu substrate and the solder, as well as inside the solidified SAC305 solder alloy, as shown in Figure 8a. At higher magnification, the surface was seen to be mostly flat, consisting of micro ductile dimples and brittle failure indicating a mixed failure that occurred in the solder of SAC305 (Figure 8d). Similar fracture behavior was also found on the other control sample with different soldering parameters. This observation is in accordance with the joint strength measurement obtained where they had approximately similar value of joint strength (Figure 7).

A rougher fractured surface was obtained on the sample soldered with P15 porous Cu, as shown in Figure 8b. Fractured form of the porous Cu interlayer was obviously detected at the broken surface after the tensile testing. This observation is similar to the brazing process involving metal foam where a cup and cone liked structure of metal foam was detected at fractured surface [26]. The failure locations were found at the solder interface close to the porous Cu interface, which corresponds to the IMC layer. This can be explained by the formation of Cu_6Sn_5 IMC phase at the boundary between the solder and porous Cu, as shown in Figure 8e. A larger solid cell wall for P15 will reduce the penetration of molten solder inside porous Cu, creating a segment unreachable by molten solder during the soldering process. Consequently, P15 bonding solid cell walls develop weakness hence explaining the observation for lower joint strength of P15 porous Cu solder joint compared to the P25 porous Cu at soldering temperatures of 267 °C and 287 °C (Figure 7a,b). However, at a higher soldering temperature (307 °C) with soldering time 60 s and 300 s, the joint strength of solder joint with P15 porous Cu obtained is slightly higher than the corresponding solder joint with P25 porous Cu.

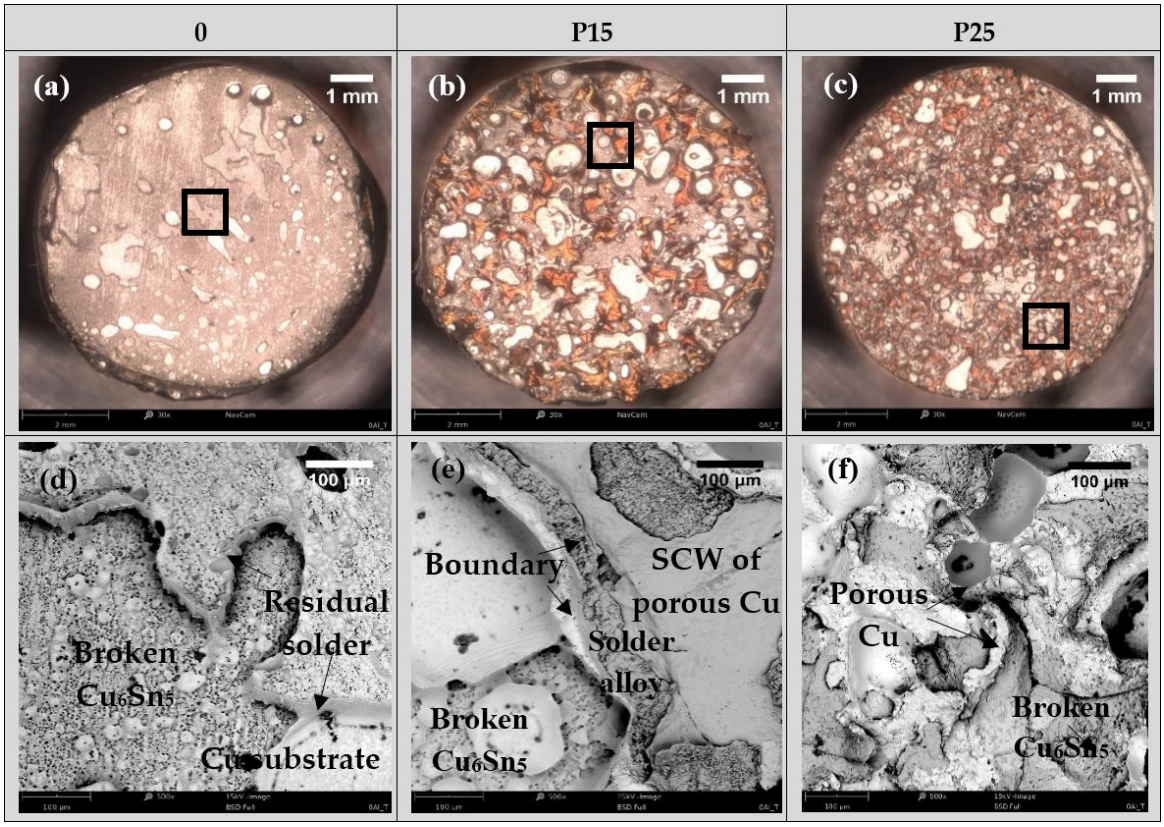

Figure 8. Fracture morphology of solder joint at soldering temperature of 307 °C with soldering time of 300 s; (**a**–**c**) optical microscope; (**d**–**f**) high magnification from SEM.

Figure 8c shows the fracture surface of the P25 porous Cu interlayer specimen. As shown in Figure 7, higher joint strength was obtained for the solder joint with P25 porous Cu. The bright dimple which arises from the cleavage surface was detected at the wall boundary of porous Cu and solder alloy (Figure 8f). This cleavage surface developed as a result of decohesion of IMC involving Cu from porous Cu and Sn from molten solder during slow elongation rate of tensile testing. As the amount of Cu atom increased in solder joint system of P25 porous Cu, the reaction of Cu-Sn increased as well to form the IMC phase. The IMC phase formation hindered the motion of atoms dislocation [27]. Subsequently, this strengthened the adhesive bonding of interfacial reaction to increase the joint strength of solder joint with P25 porous Cu, except for the solder joint formed at 307 °C with soldering time of 60 s and 300 s.

The relationship between the test load and displacement of solder joint of every sample at constant speed rate of 0.5 mm/min at room temperature is shown in Figure 9. The points marked as x_1, x_2, x_3 are the elongation distance to break the solder joint for samples without porous Cu as well as samples with P15 and P25 porous Cu, respectively. From this, it is evident that the elongation of solder joint with the addition of porous Cu increased to a larger extent compared to (without degrading the joint strength) the solder joint without porous Cu. The solder joint with higher porosity of P25 porous Cu had a larger elongation than the P15 porous Cu solder joint. The result can be summarized by the following trend: $x_3 > x_2 > x_1$. The increase of Cu atom quantity from porous Cu into interfacial reactions during solidification of molten solder leads to formation of the IMC layer. This interaction between Cu atoms and element from molten solder had possibly restricted the atom dislocation movement and thereby increased the motion resistances of the solder joint, which ultimately generated plastic behavior of the solder joint [13,27–29].

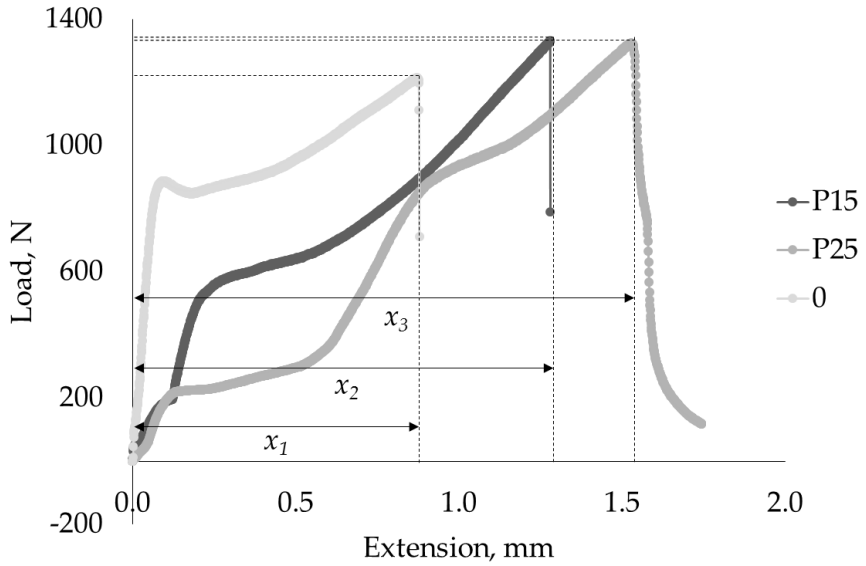

Figure 9. Load-extension curve for solder joints with and without porous Cu soldered at 307 °C with soldering time of 300 s.

3.3.2. Cross-Sectional Analysis

In order to better understand the crack behaviour of solder joint with addition of porous Cu interlayer, the cross section of an as-soldered sample and after tensile test solder joint were observed. Figure 10 shows the cross section micrograph of the solder joint with and without the porous Cu interlayer. The as-soldered condition of solder joint without porous Cu is shown in Figure 10a. It is evident that the crack initiated at the interface of IMC/SAC305 close to the Cu substrate and expanded along the interface as in Figure 10b.

In the case of solder joint with added P15 porous Cu, a large segment of solid cell walls are in contact with each other after being rolled to a very thin layer. As a result, the penetration of molten solder into porous Cu is limited by the blockage from this solid cell wall structure (Figure 10b), and so the crack fracture occurred inside the SAC305, inside the porous Cu and through the interface of porous Cu/IMC (Figure 10c). Despite the smaller pore diameter in P25 porous Cu compared to P15 porous Cu, it was evident that the solid cell walls of P25 porous Cu had less contact with each other as compared to P15 porous Cu. This facilitated better molten solder penetration to reach the inner portion of the porous structure. From Figure 10c, the penetrated molten solder filled the gap inside P25 porous Cu which was evident. It was found that a crack occurred inside the solder, and a few at IMC/SAC305 interface when stress was loaded (Figure 10f). The crack also happened inside porous Cu, which leads to a cleavage fractured, surface as mentioned in Section 3.3.1.

On the other hand, the fracture, along those interfacial boundaries, was accelerated by interfacial stress produced by the differences in physical properties such as thermal expansion. The presence of porous metal in joining assemblies evidently minimize the difference in thermal expansion between the interfaces to prevent the occurrence of joint crack [18]. Therefore, it can be concluded that the use of porous Cu with capability of residual stress absorption can enhance the bond reliability and prevent them from cracking, which was similarly mentioned by Fang et al. in their study through the use of Cu interlayer in joining assembly [17].

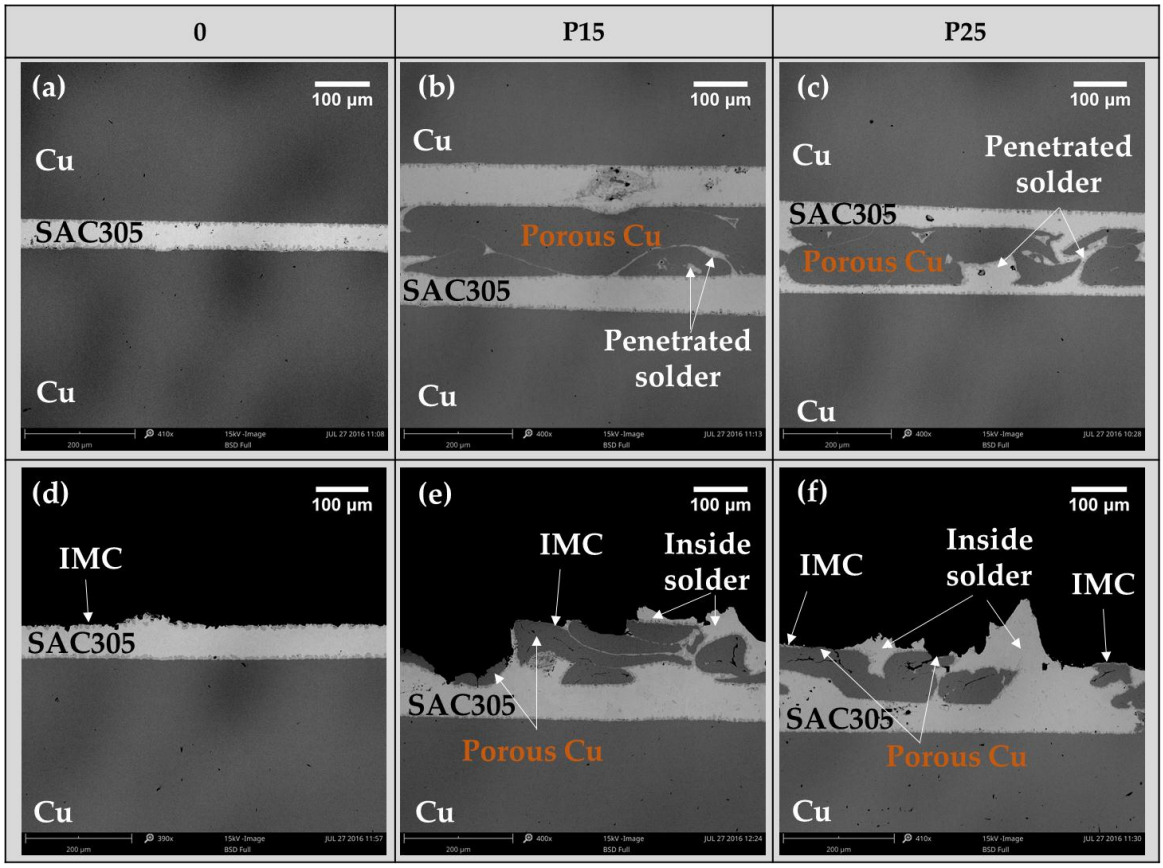

Figure 10. Cross-sectional image of solder joint at soldering temperature of 307 °C with soldering time of 300 s, (**a**–**c**) as-soldered cross section; and (**d**–**f**) after crack; for solder joint with 0, P15, and P25 porous Cu.

3.4. Interfacial Structure Analysis

The joint strength of a solder joint is greatly influenced by the metallurgical bonding layer between the solder alloy and the Cu substrate. It is a fact that the interfacial reactions that form IMC have a role to ensure the effective joining between solder/solid interfaces [30]. Figures 11 and 12 show the backscattered electron (BSE) images of IMC layers formed at both sides, namely at the substrate and porous Cu interlayer. The elements of the selected surface are listed in Table 4, together with their respective phases as identified according to the Sn-Cu phase diagram [31]. Basically, the Cu atoms of IMC phase migrated from SAC305 solder alloy and the Cu substrate to form Cu_6Sn_5 phase joining interface [32,33]. As seen in Figure 11a–c, the growth of an elongated scallop-liked layer of Cu_6Sn_5 phase at SAC305/Cu substrate interface was observed for the sample soldered at 307 °C and 300 s with and without the addition of porous Cu. A very thin layer of Cu_3Sn phase was also observed at the boundary of Cu substrate in every sample. This is probably due to the limited diffusion of Sn from Cu_6Sn_5 phase.

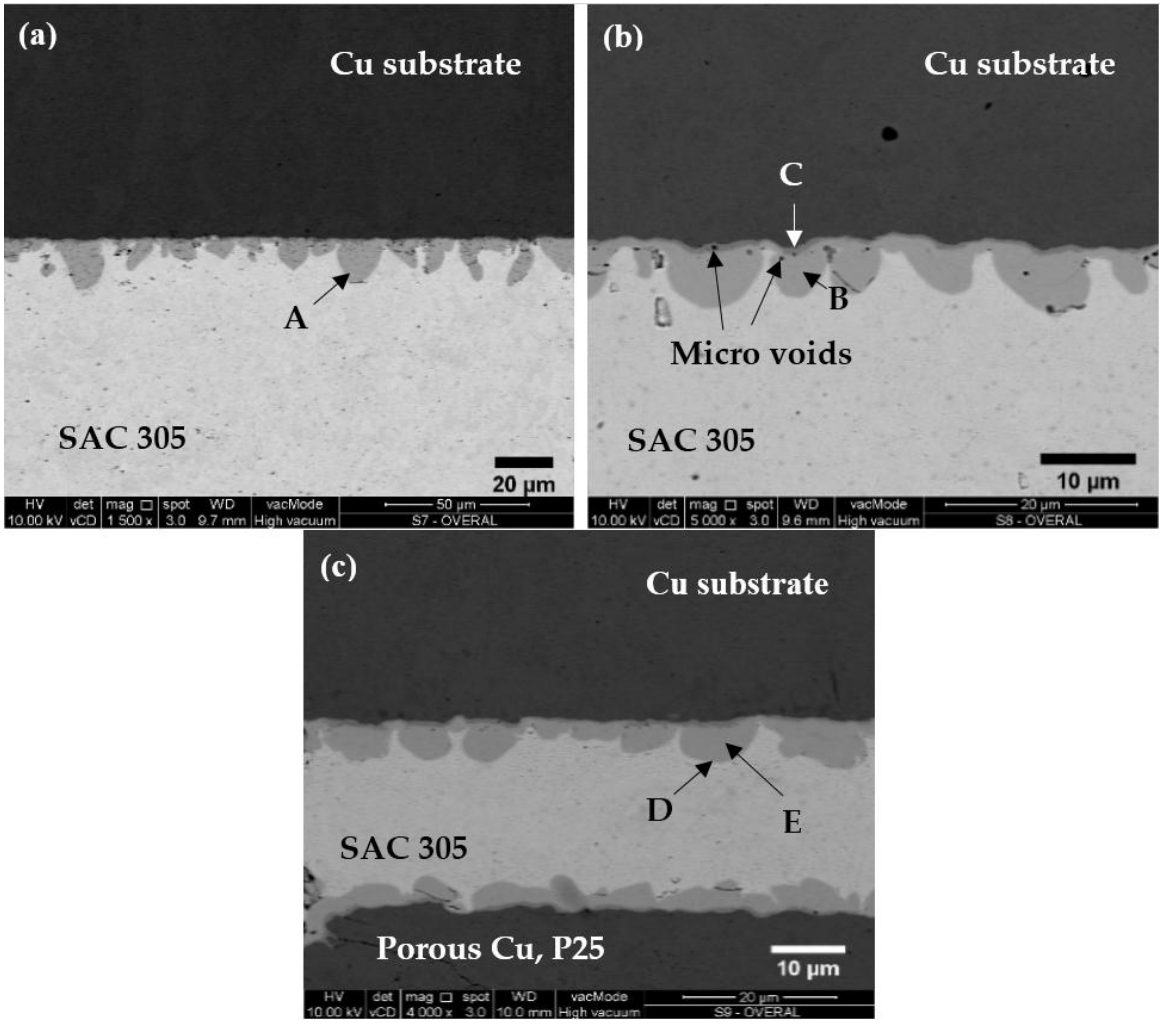

Figure 11. Formation of intermetallic compound (IMC) layer at solder/Cu substrate for solder joint soldered with (**a**) no porous Cu; (**b**) P15 and (**c**) P25 at 307 °C with a holding time of 300 s.

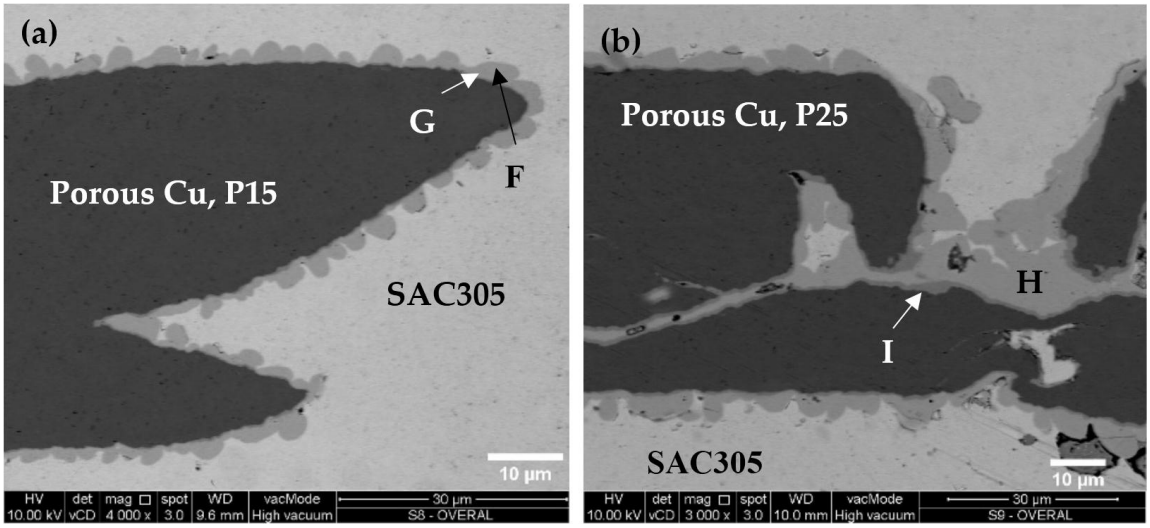

Figure 12. Formation of IMC layer at solder/porous Cu for solder joint soldered with (**a**) P15 and (**b**) P25 at 307 °C with a holding time of 300 s.

Table 4. The element atomic percentage by energy dispersive X-ray (EDX) analysis for Figures 11 and 12.

Point	Element (at. %)		
	Cu	Sn	Phase
A	55.17	44.6	Cu_6Sn_5
B	55.41	44.41	Cu_6Sn_5
C	67.19	32.77	Cu_3Sn
D	56.71	43.16	Cu_6Sn_5
E	72.33	27.67	Cu_3Sn
F	55.42	44.5	Cu_6Sn_5
G	63.4	36.32	Cu_3Sn
H	56.35	43.12	Cu_6Sn_5
I	66.25	33.5	Cu_3Sn

Alternatively, with the addition of the porous Cu interlayer, both typical scallop-liked as well as more uniform and continuous layer of Cu_6Sn_5 phases were observed. Both types of IMC phases were present in the solder joint with porous Cu, with the scallop-shaped phases found to be more dominant for P15 porous Cu solder joint, while the latter phase appeared to be more prominent for the solder joint with P25 porous Cu (Figure 12a,b). The pores of P25 porous Cu was more compressed and compacted due to its smaller solid cell wall (0.06 mm). Smaller pore diameter of P25 porous Cu provided a larger contact area for the dissolution reaction with the molten solder to form IMC Cu_6Sn_5 at porous Cu/SAC305 interface. Therefore, it can be assumed that more diffusion process of Cu-Sn atom occurred at porous Cu/SAC305 interface during penetration of molten solder into P25 porous Cu as compared to P15, leading to the formation of a more uniform and less-developed scallop type IMC structure at the solder joint with P25 porous Cu. This behavior was similarly found in Zou et al.'s investigation, where, with the use of small particles in solder alloy, had increased the surface area to volume ratio of reaction [6].

The structure of porous Cu consists of pores with varying diameter. The pores provide more channels to allow the molten solder to penetrate into the internal porous structure and therefore increase the element diffusion to provide a gripping mechanism. This results in the formation of IMC which forms an adhesion between solder and porous Cu as reported by George et al. [34].

3.5. Measurement of IMC Thickness

The shape of IMC Cu_6Sn_5 phase at the SAC305/Cu substrate is typically hemispherical [35]. Additionally, it is a known fact that solid Cu has high conductive properties. It is mostly utilized as heat exchangers for power electronics. On the contrary, porous Cu has a relatively low amount of metal and therefore possesses low thermal conductivity, which is only adequate for commercial electronics application [22]. The addition of porous Cu interlayer to the solder joint will therefore provide more contact areas for heat transfer from solder alloy during the soldering process, which forms a homogeneous IMC layer at SAC305/porous Cu interface.

Measurements on the IMC thickness at the interfaces would provide additional information that is relevant to the behavior of the solder joints. The average thickness of the IMC layer (Cu_6Sn_5, Cu_3Sn) for every sample is shown in Table 5. The thickness of IMC layer at the interface of SAC305/Cu substrate without porous Cu increased 1 µm with every increase of 20 °C of soldering temperature. For solder joint with porous Cu, the measurement was made at both interfaces of SAC305/Cu substrate and SAC305/porous Cu, and results showed that there was not much variation in the IMC thickness measurement for both the interfaces; except at 307 °C, in which the IMC thickness for P15 porous Cu at SAC305/Cu was about 2 µm thicker than at SAC305/P15 porous Cu interface. Similar observation was also noted for the IMC thickness at the solder joint with P25 porous Cu and SAC305/Cu interface. It can be deduced that the IMC thickness at SAC305/porous Cu reached the limit of deformation

around 3–5 μm. Meanwhile, the IMC thickness at SAC305/Cu substrate for solder joint with and without porous Cu showed a similar pattern of increment. This thickness measurement conformed with the readings of typical IMC layer at interface of SAC305/Cu substrate as reported elsewhere [36].

Table 5. Average thickness of intermetallic compound (IMC) layer for every sample.

Soldering Temperature, °C	IMC Thickness, μm				
	No Porous	P15		P25	
		SAC/Cu	SAC/Porous	SAC/Cu	SAC/Porous
267	4.2	3.6	3.3	4.6	3.9
287	5.0	4.8	4.1	5.5	4.4
307	6.4	6.5	4.9	6.8	4.5

4. Conclusions

The effect of porous Cu interlayer addition on the mechanical and microstructural characteristics of SAC305 solder joints formed under different soldering times and temperatures were investigated. The results obtained are summarized as follows:

(1) The joint strength of the Pb-free SAC305 solder joint with the addition of porous Cu interlayer generally increased alongside with increasing soldering time and temperature.

(2) The highest strength for the solder joint with P25 porous Cu addition was recorded at 51 MPa, at soldering time of 180 s and temperature of 307 °C, whereas the 54 MPa highest strength was achieved with P15 porous Cu addition at 300 s with 307 °C.

(3) For solder joints without porous Cu, fracture occured along the interface of solder alloy and Cu substrate. In the case of solder joints soldered with P15 and P25 porous Cu interlayer, fractures occured at three regions, namely at the interface of solder and porous Cu interlayer, inside the porous Cu interlayer as well as inside the solder itself.

(4) Microstructural analysis at the interfacial regions revealed the IMC phase at the SAC305/Cu substrate interface to have a scallop-liked configuration. With addition of porous Cu, both typical scallop-shaped as well as more uniform and continuous layers of IMC phases were observed. The typical scallop-liked configurations were more dominant for the solder joint with P15 porous Cu at the SAC305/P15 porous Cu interface, whereas the latter phase appeared to be more prominent for the solder joint with P25 porous Cu at the SAC305/P25 porous Cu interface.

(5) The IMC layer at the interface of solder alloy and Cu substrate of all specimens was thicker than that at the interface of solder alloy and porous Cu. The IMC layers at these two regions also increased with soldering temperature. The uneven contact area at the interface of porous Cu and solder alloy resulted in the formation of a less pronounced IMC layer.

Acknowledgments: The author greatly appreciated the financial support of this research by the Postgraduate Research Fund, PPP (PG129-2012B) and University Malaya Research Grant, UMRG (RP035A-15AET) from University of Malaya (Kuala Lumpur, Malaysia), Tokai University (Kanagawa, Japan), and contributions from Nagaoka University of Technology (Niigata, Japan) for their support on this study.

Author Contributions: Nashrah Hani Jamadon performed the experiments, analyzed the data and wrote the article. Ai Wen Tan played a key role in reviewing the article. Ariga Tadashi and Miyashita Yukio provided the material for the experiments and gave input on the running of the experiments. Farazila Yusof and Mohd Hamdi supervised the work and discussed the results in detail.

Conflicts of Interest: The authors declare no conflict of interest.

References

1. Suganuma, K. The Current Status of Lead-Free Soldering. *ESPEC Technol. Rep.* **2002**, *13*, 1–8.
2. Chidambaram, V.; Hattel, J.; Hald, J. High-temperature lead-free solder alternatives. *Microelectron. Eng.* **2011**, *88*, 981–989. [CrossRef]

3. Shnawah, D.A.; Said, S.B.M.; Sabri, M.F.M.; Badruddin, I.A.; Che, F.X. High-Reliability Low-Ag-Content Sn-Ag-Cu Solder Joints for Electronics Applications. *J. Electron. Mater.* **2012**, *41*, 2631–2658. [CrossRef]
4. Sabri, M.F.M.; Shnawah, D.A.; Badruddin, I.A.; Said, S.B.M.; Che, F.X.; Ariga, T. Microstructural stability of Sn-1Ag-0.5Cu-*x*Al (x = 1, 1.5, and 2 wt. %) solder alloys and the effects of high-temperature aging on their mechanical properties. *Mater. Charact.* **2013**, *78*, 129–143. [CrossRef]
5. Lejuste, C.; Hodaj, F.; Petit, L. Solid state interaction between a Sn-Ag-Cu-In solder alloy and Cu substrate. *Intermetallics* **2013**, *36*, 102–108. [CrossRef]
6. Zou, C.D.; Gao, Y.L.; Yang, B.; Xia, X.Z.; Zhai, Q.J.; Andersson, C.; Liu, J. Nanoparticles of the Lead-free Solder Alloy Sn-3.0Ag-0.5Cu with Large Melting Temperature Depression. *J. Electron. Mater.* **2008**, *38*, 351–355. [CrossRef]
7. Gayle, F.W.; Becka, G.; Badgett, J.; Whitten, G.; Pan, T.; Grusd, A.; Bauer, B.; Lathrop, R.; Slattery, J.; Anderson, I.; et al. High Temperature Lead-Free Solder for Microelectronics. *JOM* **2001**, *53*, 17–21. [CrossRef]
8. Cheng, F.; Gao, F.; Nishikawa, H.; Takemoto, T. Interaction behavior between the additives and Sn in Sn-3.0Ag-0.5Cu-based solder alloys and the relevant joint solderability. *J. Alloy. Compd.* **2009**, *472*, 530–534. [CrossRef]
9. Suganuma, K.; Kim, S.; Kim, K. High-Temperature Lead-Free Solders: Properties and Possibilities. *JOM* **2009**, *61*, 64–71. [CrossRef]
10. Chellvarajoo, S.; Abdullah, M.Z.; Samsudin, Z. Effects of Fe_2NiO_4 nanoparticles addition into lead free Sn-3.0Ag-0.5Cu solder pastes on microstructure and mechanical properties after reflow soldering process. *Mater. Des.* **2015**, *67*, 197–208. [CrossRef]
11. Chellvarajoo, S.; Abdullah, M.Z. Microstructure and mechanical properties of Pb-free Sn-3.0Ag-0.5Cu solder pastes added with NiO nanoparticles after reflow soldering process. *Mater. Des.* **2016**, *90*, 499–507. [CrossRef]
12. Liu, W.; Lee, N.-C.; Bachorik, P. An innovative composite solder preform for TLP bonding—Microstructure and properties of die attach joints. *Electron. Packag. Technol. Conf. EPTC 2013* **2013**. [CrossRef]
13. Nadia, A.; Haseeb, A.S.M.A. Effects of addition of copper particles of different size to Sn-3.5Ag solder. *J. Mater. Sci. Mater. Electron.* **2011**, *23*, 86–93. [CrossRef]
14. Degischer, H.P.; Kriszt, B. *Handbook of Cellular Metals: Production, Processing, Applications*; Wiley-VCH: Weinheim, Germany, 2002.
15. Qu, Z.; Wang, T.; Tao, W.; Lu, T. Experimental study of air natural convection on metallic foam-sintered plate. *Int. J. Heat Fluid Flow* **2012**, *38*, 126–132. [CrossRef]
16. Liu, Y.; Chen, H.F.; Zhang, H.W.; Li, Y.X. Heat transfer performance of lotus-type porous copper heat sink with liquid GaInSn coolant. *Int. J. Heat Mass Transf.* **2015**, *80*, 605–613. [CrossRef]
17. Fang, F.; Zheng, C.; Lou, H.; Sui, R. Bonding of silicon nitride ceramics using Fe-Ni/Cu/Ni/Cu/Fe-Ni interlayers. *Mater. Lett.* **2001**, *47*, 178–181.
18. Zaharinie, T.; Moshwan, R.; Yusof, F.; Hamdi, M.; Ariga, T. Vacuum brazing of sapphire with Inconel 600 using Cu/Ni porous composite interlayer for gas pressure sensor application. *Mater. Des.* **2014**, *54*, 375–381. [CrossRef]
19. Jamadon, N.H.; Miyashita, Y.; Yusof, F.; Hamdi, M.; Otsuka, Y.; Ariga, T. Formation behaviour of reaction layer in Sn-3.0Ag-0.5Cu solder joint with addition of porous Cu interlayer. *IOP Conf. Ser. Mater. Sci. Eng.* **2014**, *61*, 012020. [CrossRef]
20. Yang, K.-S.; Chung, C.-H.; Lee, M.-T.; Chiang, S.-B.; Wong, C.-C.; Wang, C.-C. An experimental study on the heat dissipation of LED lighting module using metal/carbon foam. *Int. Commun. Heat Mass Transf.* **2013**, *48*, 73–79. [CrossRef]
21. Fakpan, K.; Otsuka, Y.; Mutoh, Y.; Inoue, S.; Nagata, K.; Kodani, K. Creep-Fatigue Crack Growth Behavior of Pb-Containing and Pb-Free Solders at Room and Elevated Temperatures. *J. Electron. Mater.* **2012**, *41*, 2463–2469. [CrossRef]
22. Thewsey, D.J.; Zhao, Y.Y. Thermal conductivity of porous copper manufactured by the lost carbonate sintering process. *Phys. Status Solidi* **2008**, *205*, 1126–1131. [CrossRef]
23. Nawaz, K.; Bock, J.; Jacobi, A.M. Thermal-Hydraulic Performance of Metal Foam Heat Exchangers. Available online: http://docs.lib.purdue.edu/iracc/1283 (accessed on 7 September 2016).
24. Afendi, M.; wan Nordin, W.N.; Daud, R.; Tokuo, T. Strength and Fracture Characteristics of Shear Adhesive Dissimilar Joint. In Proceedings of the International Conference On Applications and Design in Mechnaical Engineering 2012, Penang, Malaysia, 27–28 February 2012.

25. Kim, K.S.; Huh, S.H.; Suganuma, K. Effects of fourth alloying additive on microstructures and tensile properties of Sn-Ag-Cu alloy and joints with Cu. *Microelectron. Reliab.* **2003**, *43*, 259–267. [CrossRef]
26. Shirzadi, A.A.; Zhu, Y.; Bhadeshia, H.K.D.H. Joining ceramics to metals using metallic foam. *Mater. Sci. Eng. A* **2008**, *496*, 501–506.
27. Liu, W.; Wang, C.; Tian, Y.; Chen, Y. Effect of Zn addition in Sn-rich alloys on interfacial reaction with Au foils. *Trans. Nonferrous Met. Soc. China* **2008**, *18*, 617–622. [CrossRef]
28. El-Daly, A.A.; Fawzy, A.; Mohamad, A.Z.; El-Taher, A.M. Microstructural evolution and tensile properties of Sn-5Sb solder alloy containing small amount of Ag and Cu. *J. Alloy. Compd.* **2011**, *509*, 4574–4582. [CrossRef]
29. El-Daly, A.A.; Hammad, A.E. Development of high strength Sn-0.7Cu solders with the addition of small amount of Ag and In. *J. Alloy. Compd.* **2011**, *509*, 8554–8560. [CrossRef]
30. Lee, C.C.; Wang, P.J.; Kim, J.S. Are intermetallics in solder joints really brittle? *Proc. Electron. Compon. Technol. Conf.* **2007**. [CrossRef]
31. Kattner, U.R. Phase diagrams for lead-free solder alloys. *JOM* **2002**, *54*, 45–51. [CrossRef]
32. Fallahi, H.; Nurulakmal, M.S.; Arezodar, A.F.; Abdullah, J. Effect of iron and indium on IMC formation and mechanical properties of lead-free solder. *Mater. Sci. Eng. A* **2012**, *553*, 22–31. [CrossRef]
33. Yang, M.; Cao, Y.; Joo, S.; Chen, H.; Ma, X.; Li, M. Cu_6Sn_5 precipitation during Sn-based solder/Cu joint solidification and its effects on the growth of interfacial intermetallic compounds. *J. Alloy. Compd.* **2014**, *582*, 688–695. [CrossRef]
34. George, E.; Das, D.; Osterman, M.; Pecht, M. Thermal cycling reliability of lead-free solders (SAC305 and Sn3.5Ag) for high-temperature applications. *IEEE Trans. Device Mater. Reliab.* **2011**, *11*, 328–338. [CrossRef]
35. Tan, A.T.; Tan, A.W.; Yusof, F. Influence of nanoparticle addition on the formation and growth of intermetallic compounds (IMCs) in Cu/Sn-Ag-Cu/Cu solder joint during different thermal conditions. *Sci. Technol. Adv. Mater.* **2015**, *16*, 033505.
36. Wu, C.M.L.; Yu, D.Q.; Law, C.M.T.; Wang, L. Properties of lead-free solder alloys with rare earth element additions. *Mater. Sci. Eng. R Rep.* **2004**, *44*, 1–44. [CrossRef]